An Origami-Based Cable-Climbing Robot

Juhyung Kim, Xiuxian Shi, Zifeng Wang, and Wei Dawid Wang*

***Abstract*—Cable-climbing robots are essential for performing inspection and maintenance in hard-to-reach places with a cable-based infrastructure. However, current robots are often either cumbersome, have low load capacities, or struggle to accommodate cables with largely varying diameters. To address these issues with a single design, this study demonstrates an origami-based, cable-climbing soft robot capable of caterpillar-like anchor-crawling locomotion. This robot weighs around 110 g and consists of a body mechanism and two leg mechanisms. The body mechanism with sufficient compliance can adapt to various bends of the cables. The leg mechanism utilizes a bionic gripping design that enables it to climb cables with diameters ranging from less than 1 mm to tens of millimeters. Additionally, the bistable performance of the leg mechanism allows the robot to secure itself to cables within a certain diameter range, even without continuous actuation. Moreover, the robot has a good load capacity and, for instance, can carry a load of more than ten times its weight on a vertical cable with a diameter of 30 mm. More capabilities of the robot are also demonstrated, including crawling between cables with different diameters, transporting items, and completing complex tasks, such as repairing damaged cables.**

***Index Terms*— cable-climbing robots, caterpillar-like locomotion, origami-based soft actuators, soft robots.**

I. INTRODUCTION

Cable-climbing robots are crucial for maintaining and inspecting infrastructure that relies on cables, such as power lines, suspension bridges, and communication towers. These structures often extend to great heights and remote locations, making manual inspection and maintenance dangerous, time-consuming, and costly. In particular, cables are widely used to transmit electricity, particularly ultra-high voltage cables connecting telephone poles or transmission towers. These cables can also generate electromagnetic interference (EMI) due to the high voltage they carry. By automating inspection and maintenance, cable-climbing robots enhance worker safety, reduce operational costs, and enhance efficiency, creating an urgent need for their design to assist in the inspection and maintenance of cable-supported infrastructure. However, most cable-crawling robots to date have been developed as rigid robots. These rigid robots can be used for cable-stayed bridges [1][2][3][4] and high-voltage transmission lines [5][6]. However, this type is heavy due to their rigid mechanisms, which can cause large deformation of the cables and may lead to serious accidents when slipping or falling occurs. Additionally, because these robots are electrically powered and controlled, EMI from high-voltage power lines can lead to issues with their control systems [7].

In contrast, cable-crawling soft robots made of soft materials and compliant structures offer several advantages of being lightweight, highly adaptable, and safe compared to their rigid counterparts. An electrically driven soft robot has also been designed to climb thin cables [8], but its load capacity is very low (less than 0.1 N) and it is not immune to EMI from high-voltage power lines. In contrast, non-electrically powered soft robots eliminate the necessity for cumbersome mechanical components and onboard electronic components, making them a promising option for climbing high-voltage lines. The most representative ones are the pneumatic soft robots. These robots are made of flexible elastomers, so they have good insulation properties being immune to EMI from high-voltage power lines. They consist of inflatable chambers that can be inflated or deflated by pressurized air to generate various desired deformation for locomotion [9][10][11]. Pneumatic soft robots based on different designs can achieve a variety of locomotions, such as crawling [12][13][14], tube-climbing [15][16][17], swimming [18], and jumping [19][20]. There are also rod-climbing robots inspired by the winding locomotion of snakes, but they can only climb rods within a small diameter range and have low load capacity [21]. In addition, pneumatic origami actuators are a type of soft actuator that integrates the principles of origami (i.e. paper folding) with pneumatic actuation. Pneumatic origami actuators combine the advantages of soft actuators with rigid structures, and can output large deformations and strong forces at the same time [22][23][24]. These features show that pneumatic origami actuators meet the requirements of cable-climbing robots, including those that can climb high-voltage lines. However, such robots have yet to be developed.

This study demonstrates an origami-based, pneumatic soft cable-climbing robot with potential applications of inspection and maintenance in hard-to-reach places of cable-based infrastructure. The robot consists of a body mechanism containing two symmetrically arranged body actuators and two leg mechanisms, each containing four symmetrically arranged leg actuators. All actuators are Kresling-based origami soft actuators, which can be designed to be either monostable or bistable depending on different geometries [25]. The body actuators are monostable, enabling the body

This work was supported by the National Research Foundation of Korea (NRF) funded by the Korean government (MSIT) under Grant (No. RS-2023-00210231). *(Corresponding author: Wei Dawid Wang).*

The authors are with the Department of Mechanical Engineering, Hanyang University, Seoul 04763, South Korea (e-mail: pat9905@hanyang.ac.kr; shixiuxian@hanyang.ac.kr; wangzifeng97@hanyang.ac.kr; davidwang@hanyang.ac.kr).

This article has supplementary material provided by the authors and color versions of one or more of the figures in this article are available online at http://ieeexplore.ieee.org

mechanism to have sufficient flexibility and compliance to adapt to various bends in the cables, while the leg actuators are bistable, allowing the leg mechanism through its claws to achieve quick grabbing and releasing from the cable, or to stay on the cable even without requiring continuous actuation. The leg mechanism utilizes a bionic gripping design that enables it to climb cables with diameters ranging from less than 1 mm to tens of millimeters. The coordinated motion of the body mechanism and the leg mechanisms enables the robot to achieve a caterpillar-like anchor-crawling locomotion that can reach a maximum speed of 0.81 body lengths per stride. The capabilities of the robot are also demonstrated, including crawling between cables of varying diameters, transporting items, and completing complex tasks like repairing damaged cables.

II. Robot Design and Implementation

A. Robot Design

The robot consists of a body and two identical, mirror-symmetrical leg mechanisms at each end (Figure 1A). According to the forward movement direction of the robot, the leg mechanisms are referred to as the front leg mechanism and the rear leg mechanism. Inspired by the caterpillar's prolegs that grasp branches, the robot's leg mechanism also consists of two flat-nosed claws to grasp or release cables, even those with very small diameters (Figure 1B). A soft pad is attached to each claw to increase the friction between the claw and the grasped cable. The motion of each claw is actuated by two symmetrically arranged leg actuators. Each leg actuator is composed of one paired Kresling origami unit with an opposite chirality. The paired Kresling units upon simultaneous pressurization or depressurization can achieve pure linear motion (i.e., contraction or expansion) between the two ends. Additionally, the Kresling unit can be designed to be monostable or bistable depending on the design parameters. Bistable Kresling units are used for the leg actuators to achieve quick grabbing and releasing upon depressurization or pressurization. One end of a pair of leg actuators is fixed to the frame of the leg mechanism, and the other end, that is, the movable end, is fixed to the claw. Therefore, pressurizing or depressurizing both leg actuators simultaneously can drive a single claw to translate on the slide rod through the sliding pairs. As a result, synchronously controlling the four leg actuators of a pair of claws can make a pair of claws tighten or loosen the cable.

Each leg mechanism is equipped with guide rings at both the front and back. Because the two claws of the leg mechanism no longer contact the cable after releasing the cable, guide rings are needed to prevent the robot from falling off the cable. Each guide ring is a detachable module and each ring has a breakpoint for easy placement over closed cables. The modules of the guide rings are designed with different inner diameters so that the leg mechanism can stably grasp the cable with a diameter slightly smaller than the inner diameter of the guide ring. This replaceable modular design allows for easy replacement of the guide ring, enabling the robot to crawl through cables with diameters ranging from less than 1 mm to several tens of millimeters. It is worth noting that the maximum diameter of the cable that the claw can grasp depends on the deformation of a single leg actuator, that is, the deformation of a pair of Kresling units. Therefore, by increasing the number of pairs of Kresling units within the leg actuator, the claw (with larger guide rings) can be enabled to grasp cables with much larger diameters. The robot body consists of two linear Kresling assemblies, each called a body actuator (Figure 1C). Each actuator is composed of six paired Kresling units with opposite chirality. Monostable Kresling units are used for the body actuators to achieve smooth and continuous deformation upon pressurization or depressurization and to obtain a compliant structure of the robot body. The structural flexibility of the robot body enables the robot to easily adapt to various bends in the cables (Figure 1D, Movie S1). Eventually, both ends of each body actuator are rigidly connected to the movable ends of the front and rear leg actuators, respectively, thus forming the robot structure.

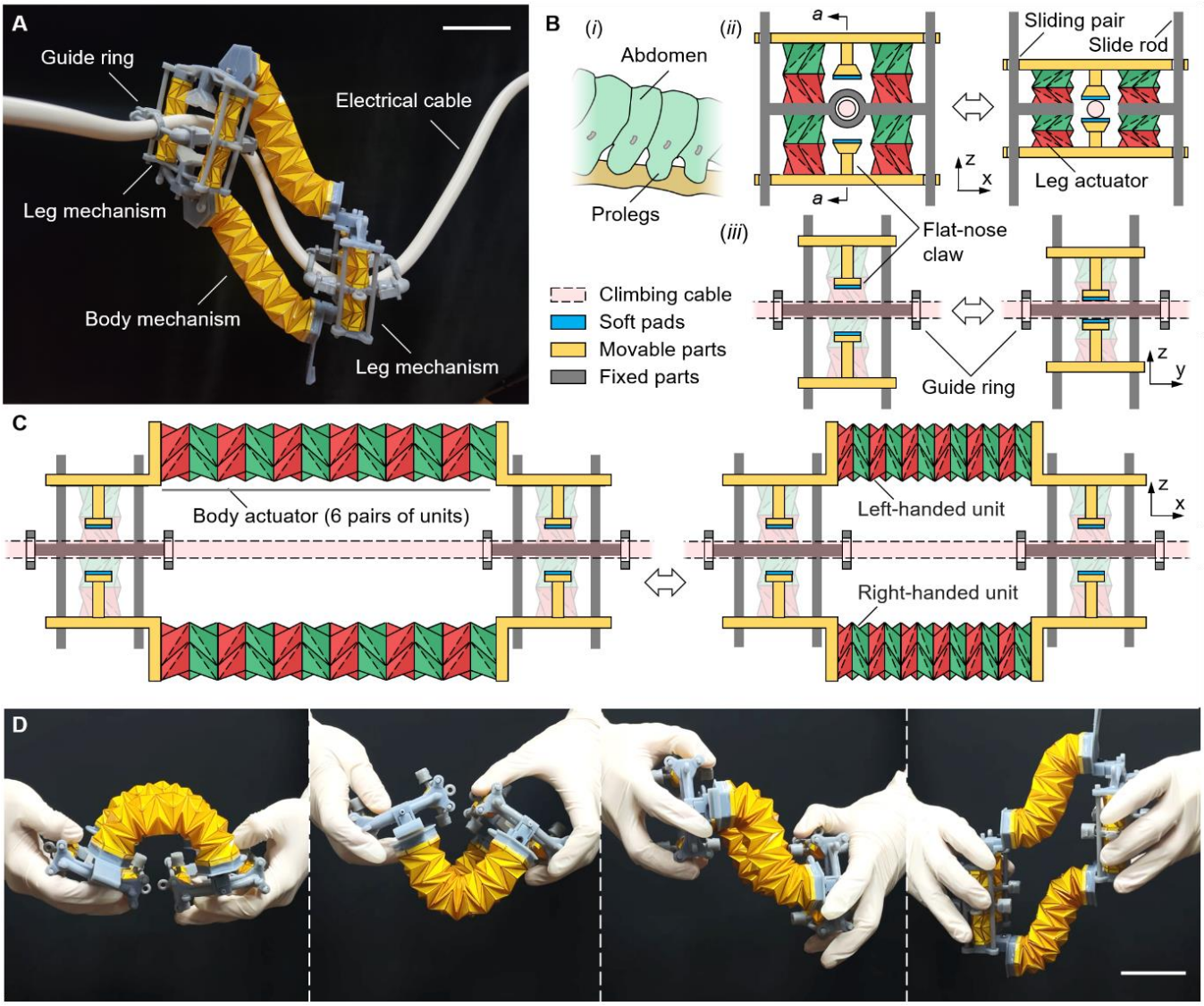

Fig. 1. Design and working principles of the cable-climbing robot. (**A**) Robot architecture with its main components. (**B**) Design of the bioinspired leg mechanism. (*i*) Schematic diagram of a caterpillar's prolegs. (*ii*) Front view of the schematic diagram of the leg mechanism grabbing (left) and releasing (right) the cable. Guide rings are not shown in the releasing state. (*iii*) Cut view along *a*-*a*. (**C**) Design of the body mechanism. The body expands when pressurized (left) and retracts when depressurized (right). The red Kresling units are left-handed, and the green ones are right-handed in (**B**) and (**C**). (**D**) Optical images of the robot at different bending states. All scale bars are 50 mm.

B. Materials and Fabrication

To fabricate an origami leg or body actuator, a polyvinyl chloride (PVC) sheet (0.2 mm thick) was first cut into identical triangles and rectangles using a cutting machine (Cameo 4, Silhouette). The dimensions of these triangles are defined by the lengths of their two shorter sides, a and b, and their included angle, β. These triangles and rectangles were then pasted to a Kapton tape (0.05 mm thick, BLEX) with an adjacent spacing of c = 1.2 mm, according to the Kresling pattern (Fig. 2A). After that, another layer of the same tape was pasted on top to form the thin-layered structure. The areas containing PVC are sandwich structures that form the facets of the Kresling units, and the areas without PVC are bonded by two layers of tape to form the creases. The layered structure is then rolled and the ends are taped together using the same tape to form a tube. Then, the Kresling-patterned origami structures are formed by manually folding the tube along the creases. The pneumatic actuators (either leg actuators or body actuators) were ultimately constructed by sealing the Kresling structure with rigid upper and lower polygonal plates made of resin (Hard tough resin, eSUN) fabricated via 3D printing (Photon Mono X, Anycubic). The side lengths of the polygonal plates of the body actuator and leg actuator are 17.3 and 8.6 mm respectively, and the corresponding areas are 777.6 and 192.1 mm^2. Moreover, previous studies have shown that when the origami actuator is unfolded to a height close to

the maximum unfoldable height, it produces an irreversible buckling deformation even under very small positive air pressures [26]. Therefore, to allow the actuator to withstand a certain positive air pressure without causing a buckling deformation, a non-stretchable, thin string, with a length less than the maximum unfoldable height of the origami actuator, is used to connect the upper and lower polygonal plates to prevent the origami actuator from unfolding to the maximum unfoldable height.

The rest of the rigid structure is also made with the same 3D printer using the same material. Finally, all the components and actuators are assembled to form the robot. The specific parameters of the robot structure are summarized and shown in Table 1. It is worth noting that the four leg actuators of each leg mechanism are interconnected with air pipes, and the two body actuators are also interconnected with air pipes, so as to achieve synchronous actuation. The desired positive pressure for the actuators is realized by controlling the compressed air through an electro-pneumatic regulator (ITV0030, SMC), and the desired negative pressure is realized by controlling the vacuum through an electronic vacuum regulator (ITV0090, SMC). The required positive and negative air pressures are applied to the designated actuators through the solenoid valves (VX220EA, SMC) to control their deformation, and then the front leg mechanism, rear leg mechanism, and the body mechanism are driven by three sets of such devices, respectively.

TABLE I
MAIN PARAMETERS OF THE ROBOT

Robot parameters	Value
Robot dimension (mm, free state)	155L × 70W × 134T
Robot dimension (mm, expanded state)	217L × 70W × 134T
Robot dimension (mm, contracted state)	92L × 70 W × 134T
Max speed (BLs per stride)	(217-92)/155 = 81%
Robot weight (g)	110

L, W, T, and BLs: length, width, thickness, and body lengths.

C. Mechanical Performance of the Origami Actuators

The body actuator was designed to be monostable, with parameters a, b, and β measuring 15.9 mm, 15.9 mm, and 120°, respectively. The monostable characteristic of the actuator is verified using a compression test where a load cell (SSM-DPN-2000N, Interface) through a universal testing machine (UTM, AGS-X Series, Shimadzu) compresses an unconstrained Kresling unit with a non-enclosed air chamber. The compressive force (i.e., the reaction force of the unit on the load cell) corresponding to the displacement is measured and recorded (Figure 2B). The results show that the reaction force remains positive throughout and does positive work. The reaction force increases fast to reach a peak value of 1.8 N at about 2 mm, then decreases slightly, and finally increases slightly again. The length of the body actuator (containing six pairs of Kresling units) is ~29 mm upon depressurization at -70 kPa and ~153 mm (constrained by an embedded string) upon pressurization at 30 kpa, with a corresponding length change of about 125 mm, that is, the length change ratio is 81% (Figure 2C). It is worth noting that the length of the embedded string is about 95% of the length of the fully inflated actuator, thereby preventing the actuator from reaching a fully inflated state to generate irreversible buckling deformation.

In contrast, the leg actuator is designed to be bistable, with parameters a, b, and β measuring 7.2 mm, 10.9 mm, and 101°, respectively (Movie S2). The bistable characteristic is verified through a similar compression test. The compressive force (i.e., the reaction force of the unit on the load cell) corresponding to the displacement was measured and recorded (Figure 2D). The compression curve separates into three distinct segments. During the first segment (i.e. the first stable state), the reaction force remains positive and does positive work. The reaction force increases fast to reach a peak value of 5.3 N at about 2 mm, and then decreases to 0 N at about 4 mm. During the second segment (i.e., the second stable state), the reaction force becomes negative and does negative work. The reaction force continues to decrease to reach a valley value of -2.7 N at about 5.5 mm, and then increases to 0 N at about 8.2 mm. In the third segment, the compression force increases from 0 N. The red highlighted portion of the curve ranging from 2.4 to 10.4 mm is the part used for the deformation of the leg actuator. Similarly, the maximum deformation of 10.4 mm from its fully expanded state is achieved by a negative pressure of -70 kPa, and the minimum deformation of 2.4 mm from its fully expanded state is caused by the restriction of the embedded string under the positive pressure. The length of each leg actuator (containing one pair of Kresling units) is ~20.7 mm (constrained by an embedded string) at a fully inflated state and ~4.7 mm at a fully contracted state, with a corresponding length change of about 16 mm (i.e., the maximum stroke of each claw) with a length change ratio of 77% (Figure 2E).

The leg actuator's first stable state allows the maximum opening of the two claws to be 32 mm to accommodate the high-voltage wires whose diameters are usually between 20 and 30 mm (Figure 2E). The actuator's second stable state allows the leg mechanism's claws to fully close or anchor on a cable of a specific diameter without the requirement of continuous actuation of the leg actuators. To anchor on the cable, the negative forces generated by the leg actuator are applied to the cable through the claws as normal forces, thus providing a resultant friction force greater than its gravity or the component of gravity along the cable. Based on a friction coefficient of 0.8, experiments show that the robot can anchor on vertical cables with diameters between 16 and 22 mm. Figure 2G shows the robot anchoring on cables with diameters of 16 and 22 mm, respectively. It is worth noting that the maximum diameter of the cable that the claw can grasp depends on both the opening size of the claws and the inner diameter of the guide ring. Therefore, by increasing the

number of pairs of Kresling units within the leg actuator and the diameter of the guide ring, the claw can be enabled to grasp cables with much larger diameters.

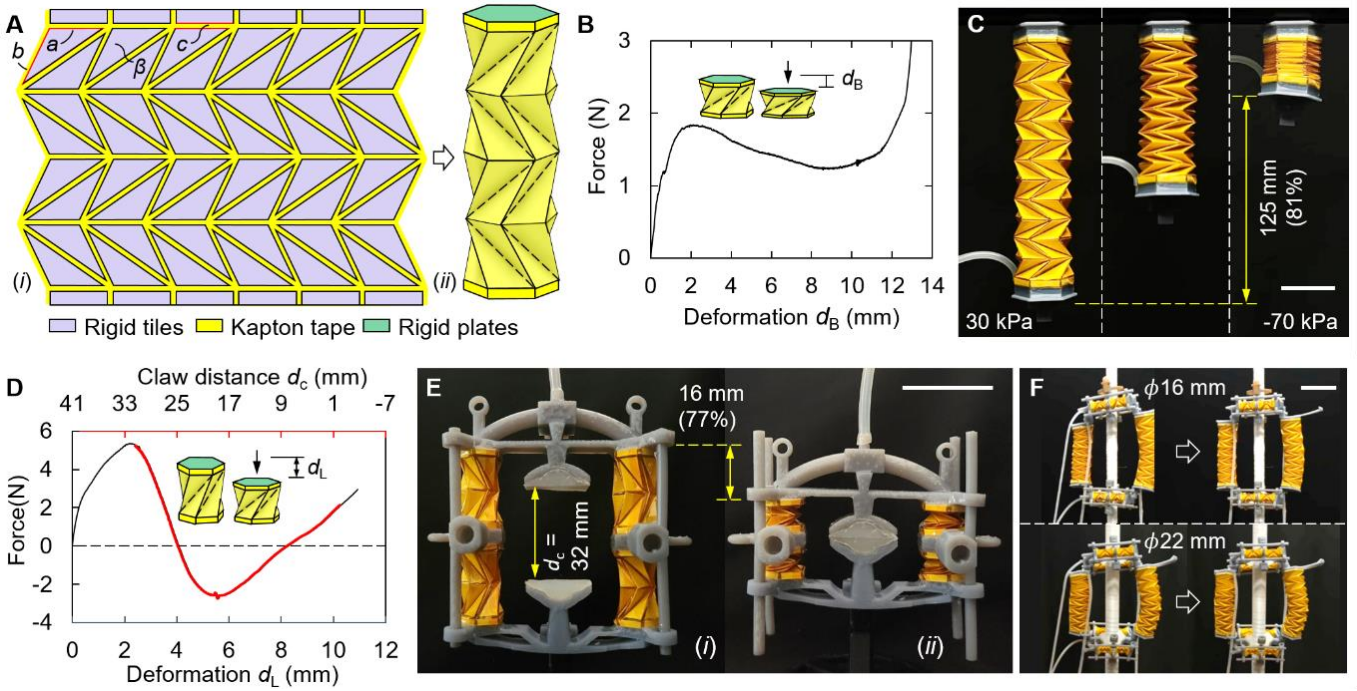

Fig. 2. Design and performance evaluations of the origami actuators. (**A**) Planar pattern of a four-unit hexagonal Kresling assembly. (*i*) The rigid pieces (in light purple) are evenly adhered to the flat tape (in yellow) with their distances from each other being consistent. (*ii*) Schematic diagram of the corresponding Kresling assembly with the added rigid upper and lower polygonal plates (in green). (**B**) Axial compression performance of a single Kresling unit of the body actuator. (**C**) Fully expanded state of a fabricated body actuator under positive pressure (30 kPa), and its fully contracted state under negative pressure (-70 kPa). (**D**) Axial compression performance of a single Kresling unit for the leg actuator. (**E**) Open and closed states of the leg mechanism. (**F**) Robot anchoring on vertical cables with diameters of 16 and 22 mm without continuous actuation of the leg actuators. All scale bars are 30 mm.

C. Locomotion Performance

The robot's motion is based on the anchor-motion crawling principle, similar to that of some caterpillars. To complete a stride, the robot needs to use its front and rear legs sequentially for anchoring (tightening the cable) during body contraction and expansion. That is, one stride of the robot consists of two main processes: anchor-pull and anchor-push. The performance of the linear locomotion was conducted on a cable with a diameter of 13 mm (Figure 3A, Movie S3). The actuation pattern with a single stride of 8 s is illustrated in Figure 3B. The period is set to 8 s to demonstrate the robot's motion, but it can be shorter if the actuator is inflated or deflated more quickly. Each stride can be divided into four sub-steps mainly of (i) anchor-anchor, (ii) anchor-push, (iii) anchor-anchor, and (iv) anchor-pull. Initially, the robot holds onto the cable with both its front and rear legs in an anchoring state. Then, the actuators in the front legs are inflated to release the cable from the front leg. Then, the body actuators are inflated to extend the body while simultaneously pushing the front leg forward. After that, the actuators in the front leg are deflated again, allowing the front leg to re-grasp the cable. Next, the actuators in the rear leg are inflated to release the cable from the rear leg. Finally, the body actuators are deflated to contract the body while simultaneously pulling the rear leg forward; this process completes the motion of one stride. It is worth noting that the front leg and the back leg cannot release the cable at the same time to prevent the robot from sliding or rotating along the cable. Figure 3C shows that the robot moved for three strides for a total distance of about 380 mm with an average speed of 0.81 BLs per stride. The robot can also crawl cables with diameters ranging from very small (even less than 1 mm) to the maximum opening size of its two claws. Figure 3D shows the robot crawling on cables with a diameter of 0.5 mm and 32 mm. In addition, Figure 3F illustrates the transition of the robot between cables with diameters of 0.5 mm and 32 mm (Movie S4).

The flexibility and compliance of the robot's body structure make the robot suitable for crawling on curved cables (Figure 4A). To test this ability, experiments were conducted to enable the robot to crawl through a 13 mm diameter cable with a 120° bend. The transition section of the cable is an arc with different bending radii. The experimental results show that the minimum curvature radius that the robot can successfully crawl through is ~34 mm (Figure 4B, Movie S5). This

minimum radius depends on the overall size of the robot and the distance between the two guide rings of the same leg mechanism. If these dimensions are reduced, the robot will be able to cross a smaller radius of curvature.

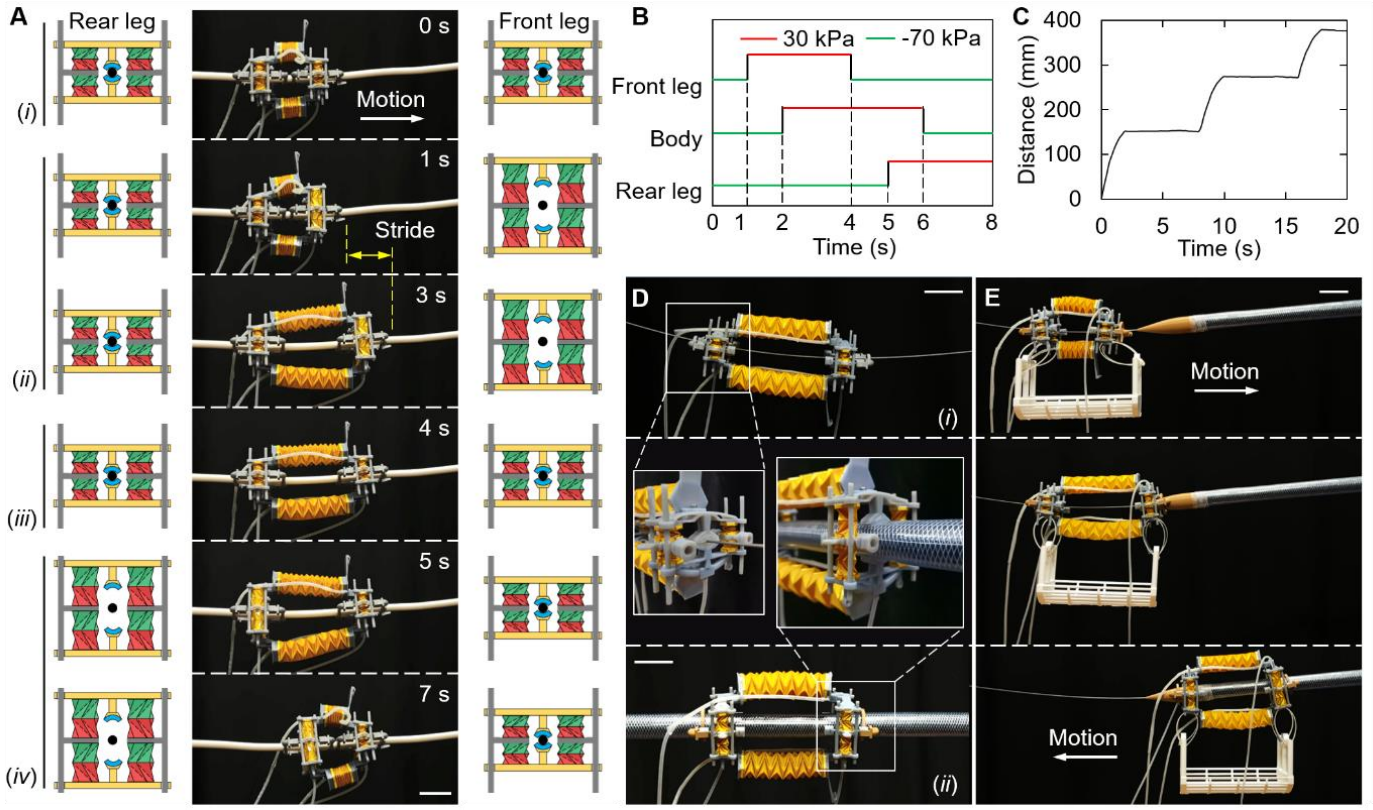

Fig. 3. Motions of the robot on straight cables. (**A**) Linear locomotion for one period. The back and front view show the configuration of the legs at each step throughout the stride. (**B**) Control patterns for linear locomotion during one period. (**C**) Linear motion performance for three strides. (**D**) Robot crawling on cables with a diameter of 0.5 mm (*i*) and 32 mm (*ii*). The insets show the robot's claws grasping the corresponding cable. (**E**) Transition of the robot between cables with diameters of 0.5 mm and 32 mm. All scale bars are 50 mm.

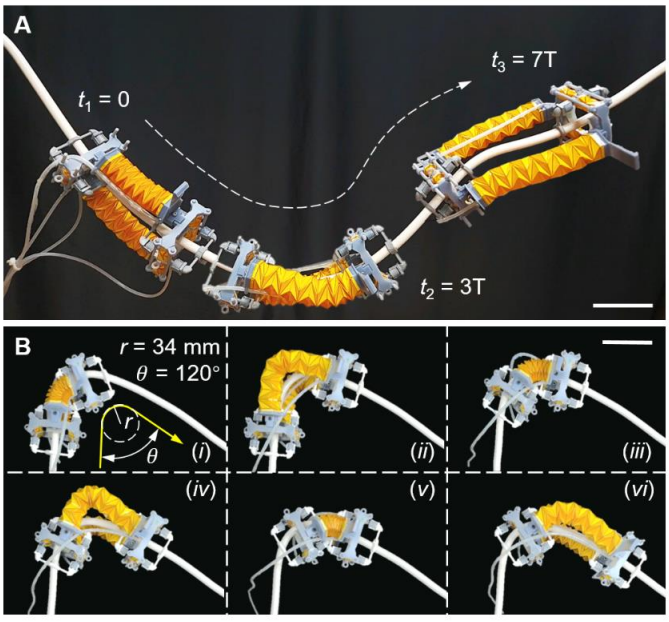

Fig. 4. Motions of the robot on curved cables. (**A**) Robot motion on a curved cable. Air tubes are not shown on the robot except in its starting position. (**B**) Motion along a 120° curve with a transition radius of about 34 mm. All scale bars are 100 mm.

D. Payload Performance on Vertical Cables

The robot's load capacity in the most challenging vertical direction depends on the contraction forces provided by the two body actuators on the one hand and the friction provided by a single leg mechanism on the other. All these forces are related to the axial force generated by a Kresling unit, therefore; a simple model based on the geometries was built to calculate the axial force under the applied pressure (Figure 5A). The two identical hexagonal bases and a kresling unit form a closed cavity, and θ = 60° is the central angle corresponding to one side of the hexagon. Moreover, R, the radius of the hexagonal base, is 8.6 and 15.9 for the body actuator and leg actuator, respectively. Based on these fabrication parameters, the initial staggered angle α_0 between the upper and lower hexagonal bases is 29° and 16.5° for units forming the body and leg actuators, respectively. The value of

α describes the rotation of the upper hexagonal base with respect to the bottom one. Since the minimum cross section in the *x*-*y* plane of the middle cavity between the upper and lower bases is still a hexagon with side length *m*, the axial force F_a of the Kresling unit under the action of applied pressure P_a can be expressed as

$$F_a = C_a P_a A_c \quad (1)$$

where $A_c = 3\sqrt{3}m^2/2$ is the area of the minimum cross-section of the cavity, and C_a is the correction coefficient to account for the error caused by the transformation of the mountain and valley creases into a curved surface [16]. The coefficient C_a is determined to be 1.9 for the current design by
fitting modeling data to experimental data. To solve the side length *m*, as shown in Fig. 5Aiii, in isosceles ΔACD,

$$\angle ACD = \angle BCD + \angle ACB = \theta + \alpha_0 + \alpha \quad (2)$$

$$\angle CAD = \angle CAF = \frac{\pi}{2} - \frac{\alpha + \alpha_0 + \theta}{2} \quad (3)$$

and in ΔAFC,

$$\angle AFC = \frac{\pi}{2} + \frac{\theta}{2} \quad (4)$$

Then, based on the law of sines in ΔAFC, the side length m can be calculated as follows

$$m = \overline{CF}_{xy} = \frac{2\sqrt{3}R}{3} \cdot \cos\frac{\theta + \alpha_0 + \alpha}{2} \quad (5)$$

where $\overline{CF}_{xy}$ represents the length of the projection of the line connecting vertices C and F in the *x*-*y* plane. It is worth noting that the force generated by the crease of the origami unit is ignored because this force is much smaller than the axial force generated by the applied pressure.

As the Kresling unit contracts, the projected area of its internal cavity continues to decrease, so that the contraction force generated under constant negative pressure continues to decrease. Related experiments were also conducted. Figure 5B shows the contraction force generated by a Kresling unit (of the body actuator) at -70 kPa. The results showed that even when the actuators were fully compressed at about 2.5 mm, the unit could still generate a minimum contraction force of approximately 30 N. Figure 5C shows the contraction force of two pairs of Kresling units at -70 kPa that actuate a claw. As the units contract, the contraction force decreases, which means that the gripping force decreases as the distance between the two claws decreases. When the contraction of units reaches 2.4 mm (that is, when the two claws are fully closed), the contraction force can still reach 5 N, making it possible for the claws to grasp thin cables with a diameter of less than 1 mm.

The friction force that the leg mechanism can provide depends on both the contraction force that the leg actuators can provide and the coefficient of friction (COF) between the claw and the grasped cable. The friction generated by a single leg mechanism at a negative pressure of -70 kPa on cables of different diameters was measured (Figure 5D).

In this experiment, to easily obtain gripping objects of different diameters and made of the same material (to achieve a uniform COF), the cables were replaced with 3D-printed rods made of polylactide (PLA) via 3D printing. Since the COF between the claw and the grasped cable plays a crucial role, the static COF of the material of the claw pad (Ecoflex 0050) to the printed PLA surface was measured to be approximately 0.67 according to the ASTM D1894 standard. The friction experiment was conducted where a leg mechanism holds a vertical fixed rod, and then the same load cell is used to pull the leg mechanism upward through inelastic strings until it slides on the rod. Rods with diameters between 1 mm and 30 mm were measured. The maximum pulling force, i.e., the maximum friction force, recorded by the load cell during this process is defined as the tangential grasping force (Figure 5E). Results show that when the same air pressure (e.g., -70 kPa) is applied, the generated maximum friction force by the leg mechanism increases with the increase in the diameter of the rod being grasped. It is worth noting that the friction force generated on a 30 mm diameter rod is 12.5 N, which is about 11 times the weight of the robot. In addition, a force of 1.4 N can still be achieved when grasping a rod with a diameter of 1 mm. The robot's climbing performance was verified by crawling on a cable with a diameter of 1 mm while carrying a load of 30 g and a cable with a diameter of 32 mm with a load of 1 kg (Movie S6).

D. Application Demonstrations

An essential use of cable-climbing robots is to transport necessary items to a designated location. Figure 6A shows the robot being used to transport a toolbox (Movie S7). By leveraging the friction between the robot's claws and the cable, the robot is still able to transport some heavy objects on the vertical cable. When the leg actuator is actuated at -70 kPa, the maximum weight that the robot can carry during climbing is around 1.2 kg (Figure 6B). The robot can also perform more complex tasks, such as repairing broken electrical wires. To accomplish this task, a camera was added to the front leg mechanism to find broken sections of wires. Moreover, a new module of the repairing module is connected to the robot via a link with unconstrained revolute joints at both ends (Figure 6C, 6D). The mechanism of the repairing module is the same as the leg mechanism, except that the soft pads of the claws are replaced by repairing covers. The cover features two types of adhesive: one with weaker adhesion on the dorsal side, allowing it to stick to the claw, and another with stronger adhesion adhesive on the ventral side. This asymmetric design allows the repairing covers to detach easily from the claws and adhere firmly to the damaged area of the cable when the repairing module presses against the damaged point of the cable with its claws. Figure 6E shows the process of locating and repairing one damaged point on a cable (Movie S8).

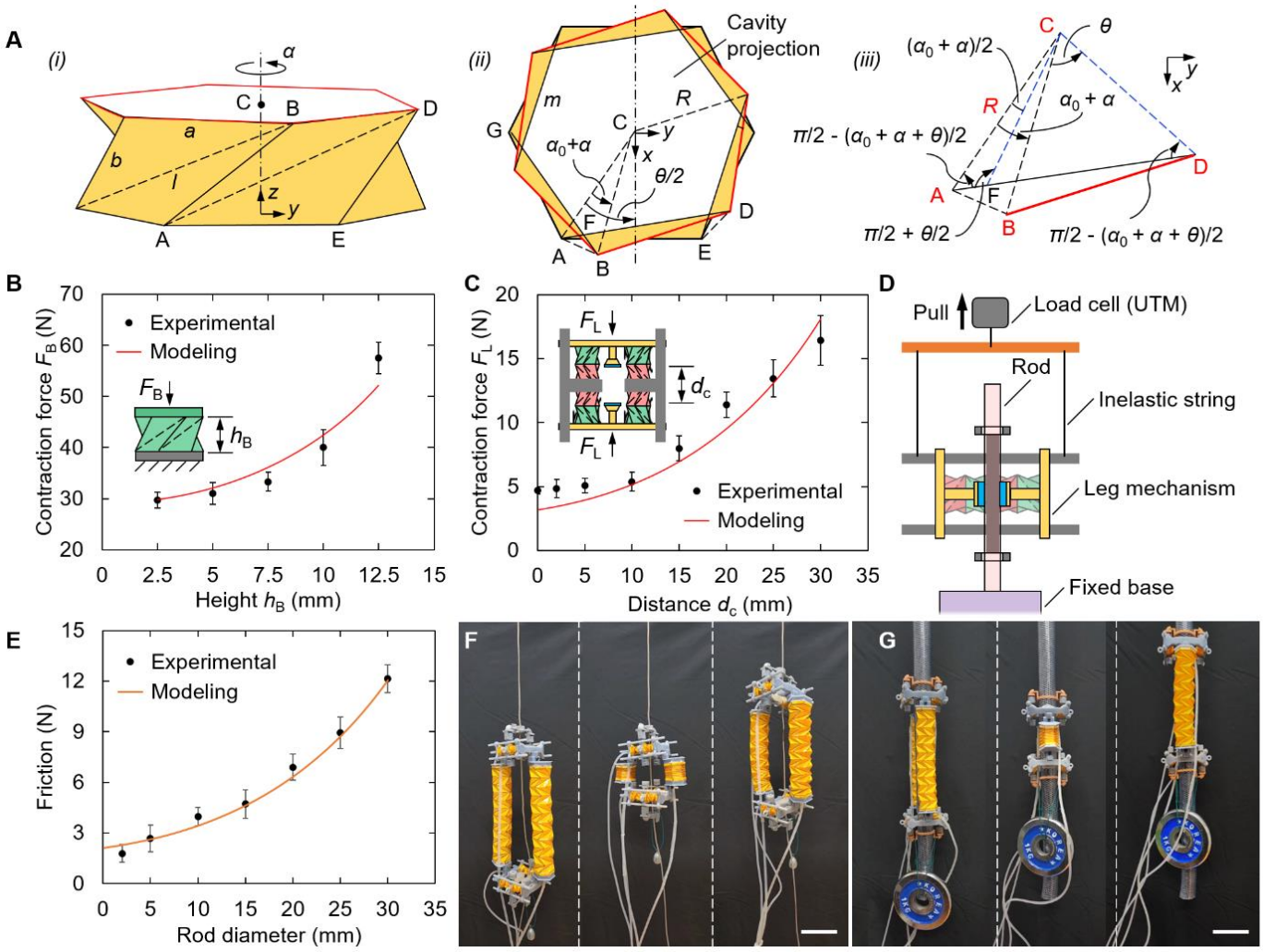

Fig. 5. Payload capacity of the robot on vertical cables. (**A**) Geometries of one Krisling origami unit. (*i*) Oblique view of the Kresling unit. (*ii*) Top-down view of the Kresling unit. (*iii*) Geometric diagram projected onto the *x*-*y* plane. (**B**) Contraction force generated by a Kresling unit of the body actuator at -70 kPa. (**C**) Contraction force of two pairs of Kresling units at -70 kPa that actuate a claw. (**D**) Schematic diagram of the experimental setup for testing the maximum friction generated by a leg mechanism on a vertical cable or rod. (**E**) Maximum friction force, that is, the tangential grasping force, generated by the leg mechanism rods with different diameters at an applied air pressure of -70 kPa. (**F**) Climbing a 1 mm diameter cable with a payload of 30 g. (**G**) Climbing a 32 mm diameter cable with a payload of 1 kg. All scale bars are 50 mm.

III. Conclusions

This study demonstrates an origami-based, pneumatic soft cable-climbing robot capable of realizing caterpillar-like anchor-crawling locomotion with a maximum moving speed of 0.81 BLs per stride. The cable-climbing robot is composed of one body mechanism and two leg mechanisms making possible several potentially useful capabilities. First, the body mechanism consisting of two parallel monostable origami actuators has sufficient compliance to adapt to various bends of the cables. Second, the leg mechanism utilizes a bionic gripping design that enables it to climb vertical cables of largely varying diameters, ranging from less than 1 mm to tens of millimeters. Third, the bistable characteristic of the leg mechanism allows the robot to attach itself to cables within a specific diameter range without requiring actuation. Fourth, the main structure of the robot (with its operating fluid being air) is made entirely of insulating materials, including polymers and elastomers, so the robot is not affected by EMI from high-voltage power lines. Fifth, it is lightweight (~110 g) and only adds minimal load to the cables, without causing any significant deformation or shaking of the cables. Sixth, the robot is modularly designed and can be easily disassembled and assembled, which enables it to be easily installed on the targeted cable. Furthermore, the robot has a high load capacity (more than 10 times its weight when climbing a 32 mm diameter vertical cable). In addition, different functional modules can be added to the robot, enabling it to perform more complex tasks, such as repairing damaged wires. Lastly, the robot is flexible and therefore harmless to humans, giving it the potential to be used with humans.

ACKNOWLEDGMENT

The authors thank J.C. for support in awarding the project.

REFERENCES

[1] F. Xu, X. Wang, and L. Wang, "Cable Inspection Robot for Cable-Stayed Bridges: Design, Analysis, and Application," *J. F. Robot.*, vol. 28, no. 3, pp. 441–459, 2011, doi: 10.1002/rob.

[2] Z. Wang, B. He, Y. Zhou, K. Liu, and C. Zhang, "Design and Implementation of a Cable Inspection Robot for Cable-Stayed Bridges," *Robotica*, vol. 39, no. 8, pp. 1417–1433, 2021, doi: 10.1017/S0263574720001253.

[3] Z. Zheng and N. Ding, "Design and implementation of CCRobot-II: A palm-based cable climbing robot for cable-stayed bridge inspection," *IEEE Int. Conf. Robot. Autom.*, vol. May 20-24, pp. 9747–9753, 2019, doi: 10.1109/ICRA.2019.8793562.

[4] H. Mengqi, J. Li, F. Xu, and L. Hu, "Design and implementation of a novel wheel-based cable inspection robot," *IEEE/RSJ Int. Conf. Intell. Robot. Syst.*, vol. 14-18 Octo, pp. 1310–1315, 2024, doi: 10.1109/IROS58592.2024.10802131.

[5] X. Yue, H. Wang, and Y. Jiang, "A novel 110 kV power line inspection robot and its climbing ability analysis," *Int. J. Adv. Robot. Syst.*, vol. 14, no. 3, pp. 1–10, 2017, doi: 10.1177/1729881417710461.

[6] P. L. Richard *et al.*, "Inside LineRanger: Mechanism Design to Optimize Operation and Performances of Powerline Inspection Robot," *IEEE Int. Conf. Robot. Autom.*, vol. 23-27 May, pp. 8157–8163, 2022, doi: 10.1109/ICRA46639.2022.9811366.

[7] W. Jiang, X. Qian, C. Tang, J. Liang, K. Zhu, and F. Lin, "Research on Electromagnetic Protection of Grounding Wire Repair Robot," *2023 6th Asia Conf. Energy Electr. Eng. ACEEE 2023*, vol. 21-23 July, pp. 171–182, 2023, doi: 10.1109/ACEEE58657.2023.10239643.

[8] W. Ma, B. Li, L. Jiang, Y. Wu, R. Bai, and G. Chen, "A Soft, Centimeter-Scaled, Thin-Cable-Crawling Robot for Narrow Space Inspection," *Adv. Intell. Syst.*, vol. 6, no. 6, pp. 1–9, 2024, doi: 10.1002/aisy.202300828.

[9] B. Mosadegh *et al.*, "Pneumatic networks for soft robotics that actuate rapidly," *Adv. Funct. Mater.*, vol. 24, no. 15, pp. 2163–2170, 2014, doi: 10.1002/adfm.201303288.

[10] H. Lee and H. Rodrigue, "Harnessing the nonlinear properties of buckling inflatable tubes for complex robotic behaviors," *Mater. Today*, vol. 63, pp. 59–88, 2023, doi: 10.1016/j.mattod.2023.02.005.

[11] W. D. Wang, W. Hu, and Z. Li, "A Physically Intelligent, Multimodal Universal Soft Gripper Using Granular Materials," *Adv. Funct. Mater.*, p. 2418549, 2025, doi: 10.1002/adfm.202418549.

[12] X. Ai, H. Yue, and W. D. Wang, "Crawling Soft Robot Exploiting Wheel-Legs and Multimodal Locomotion for High Terrestrial Maneuverability," *IEEE Trans. Robot.*, vol. 39, no. 6, pp. 4230–4239, 2023, doi: 10.1109/TRO.2023.3299530.

[13] D. Drotman, S. Jadhav, D. Sharp, C. Chan, and M. T. Tolley, "Electronics-free pneumatic circuits for controlling soft-legged robots," *Sci. Robot.*, vol. 6, no. 51, p. eaay2627, 2021, [Online]. Available: https://robotics.sciencemag.org/lookup/doi/10.1126/scirobotics.aay2627.

[14] H. Yang, S. Jin, and W. D. Wang, "Modular Assembly of Soft Machines via Multidirectional Reclosable Fasteners," *Adv. Intell. Syst.*, vol. 4, no. 7, p. 2200048, 2022, doi: 10.1002/aisy.202200048.

[15] M. S. Verma, A. Ainla, D. Yang, D. Harburg, and G. M. Whitesides, "A Soft Tube-Climbing Robot," *Soft Robot.*, vol. 5, no. 2, pp. 133–137, 2018, doi: 10.1089/soro.2016.0078.

[16] J. Liu, G. Ma, Z. Ma, and S. Zuo, "Origami-inspired soft-rigid hybrid contraction actuator and its application in pipe-crawling robot," *Smart Mater. Struct.*, vol. 32, no. 6, p. 065015, 2023, doi: 10.1088/1361-665X/acd0e7.

[17] Y. Tago, Y. Satake, and H. Ishii, "A Novel Soft Climbing Robot with Pneumatic Extendible Arms," *IEEE Robot. Autom. Lett.*, vol. 9, no. 10, pp. 8667–8673, 2024, doi: 10.1109/LRA.2024.3444669.

[18] J. Wu, M. Wu, W. Chen, C. Wang, and G. Xie, "Multimodal Soft Amphibious Robots Using Simple Plastic-Sheet-Reinforced Thin Pneumatic Actuators," *IEEE Trans. Robot.*, vol. 40, pp. 1874–1889, 2024, doi: 10.1109/TRO.2024.3360961.

[19] B. Gorissen, D. Melancon, N. Vasios, M. Torbati, and K. Bertoldi, "Inflatable soft jumper inspired by shell snapping," *Sci. Robot*, vol. 5, p. eabb1967, 2020, doi: 10.1126/scirobotics.abb1967.

[20] M. Li, H. Zhang, W. Fang, J. Wu, and X. Q. Feng, "Directional soft jumper by harnessing asymmetric snapping of a semi-open shell," *Extrem. Mech. Lett.*, vol. 72, p. 102242, 2024, doi: 10.1016/j.eml.2024.102242.

[21] B. Liao *et al.*, "Soft Rod-Climbing Robot Inspired by Winding Locomotion of Snake," *Soft Robot.*, vol. 7, no. 4, pp. 500–511, 2020, doi: 10.1089/soro.2019.0070.

[22] D. Rus and M. T. Tolley, "Design, fabrication and control of origami robots," *Nat. Rev. Mater.*, vol. 3, pp. 101–112, 2018, doi: 10.1038/s41578-018-0009-8.

[23] Z. Li, Z. Wang, and W. D. Wang, "Constrained Origami Artificial Muscle-Driven Robotic Manipulator Capable of Coordinating Twisting and Grasping Motions for Object Manipulation," *ACS Appl. Mater. Interfaces*, vol. 16, no. 6, pp. 7850–7859, 2024, doi: 10.1021/acsami.3c17978.

[24] J.-G. Lee and H. Rodrigue, "Design and Analysis of Reconfigurable Origami-Based Vacuum Pneumatic Artificial Muscles for Versatile Robotic System," *Soft*

Robot., vol. 11, no. 6, pp. 984–993, Apr. 2024, doi: 10.1089/soro.2023.0050.

[25] S. Zang, D. Misseroni, T. Zhao, and G. H. Paulino, "Kresling origami mechanics explained: Experiments and theory," *J. Mech. Phys. Solids*, vol. 188, p. 105630, 2024, doi: 10.1016/j.jmps.2024.105630.

[26] J. Zhang and C. Wang, "Deployment behavior and mechanical property analysis of Kresling origami structure," *Compos. Struct.*, vol. 341, p. 118234, 2024, doi: 10.1016/j.compstruct.2024.118234.

Juhyung Kim received the B.S. degree in mechanical engineering from Hanyang University, Seoul, South Korea, in 2025.

His research interests include soft robotics and bioinspired robotics.

Xiuxian Shi received the B.S. degree in mechanical engineering from Yanshan University, Qinhuangdao, China, in 2019, and the M.S. degree from Hanyang University, Seoul, South Korea. She is currently working toward the Ph.D. degree in mechanical engineering with Hanyang University, Seoul, South Korea.

His research interests include soft robotics and bioinspired robotics.

Zifeng Wang received the B.S. degree in mechanical engineering from Hanyang University, Seoul, South Korea, in 2021. He is currently working toward the Ph.D. degree in mechanical engineering with Hanyang University, Seoul, South Korea.

His research interests include soft robotics and bioinspired robotics.

Wei Dawid Wang received the B.S. and M.S. degrees in mechanical engineering from Harbin Institute of Technology, Harbin, China, in 2008 and 2011, and the Ph.D. degree in mechanical engineering from Seoul National University, Seoul, South Korea, in 2016. He is currently an Associate Professor with the Department of Mechanical Engineering, Hanyang University, where he directs the Soft Robotics Laboratory. His main research interests are soft robotics, bioinspired robots, smart materials and structures, and bio-inspired robotic materials